The Astronomical Journal, 124:3325–3335, 2002 December
© 2002. The American Astronomical Society. All rights reserved. Printed in U.S.A.

STRUCTURE AND DYNAMICS OF CANDIDATE O STAR BUBBLES IN N44

Yaël Nazé,[1,2] You-Hua Chu,[3,4] Martín A. Guerrero,[3,4] M. S. Oey,[5] Robert A. Gruendl,[3] and R. Chris Smith[6]

Received 2002 July 11; accepted 2002 August 21

ABSTRACT

Dynamical studies of superbubbles and Wolf-Rayet ring nebulae show discrepancies from the standard adiabatic model for windblown bubbles. We therefore study the physical properties and kinematics of three candidate bubbles blown by single O stars to evaluate whether these discrepancies are also found in these simpler objects. Our sample candidates are N44 F, N44 J, and N44 M, in the outskirts of the H II complex N44 in the Large Magellanic Cloud. We have obtained ground-based and *Hubble Space Telescope* emission-line images and high-dispersion echelle spectra for these objects. From the Hα luminosities and the [O III]/Hα ratios of these nebulae, we estimate the spectral types of the ionizing stars to be O7 V, O9.5 V, and O9.5 V for N44 F, N44 J, and N44 M, respectively. We find that the observed expansion velocity of 12 km s^{-1} for N44 F is consistent with the stellar wind luminosity expected from the central ionizing star, as predicted by the standard bubble model. The observed upper limits for the expansion velocities of N44 J and N44 M are also compatible with the expected values, within the uncertainties. We also report the discovery in N44 F of strongly defined dust columns, similar to those seen in the Eagle Nebula. The photoevaporation of these dense dust features may be kinematically important and may actually govern the evolution of the shell. The inclusion of photoevaporation processes may thus undermine the apparent agreement between the observed bubble dynamics and the simple adiabatic models.

Key words: H II regions — ISM: bubbles — ISM: individual (N44) — ISM: kinematics and dynamics — Magellanic Clouds

1. INTRODUCTION

Mechanical feedback from massive stars is a fundamental driver of galaxy evolution. The supernovae (SNe) and supersonic stellar winds from these stars generate bubbles and shells in the interstellar medium (ISM), which may dominate the ISM structure formation in many star-forming galaxies. The standard adiabatic model for these shells and superbubbles (e.g., Weaver et al. 1977) predicts the production of hot, 10^6–10^7 K, low-density gas within these shells, which bear the products of SN and massive star nucleosynthesis. Therefore, these bubble structures are thought to be the source of the diffuse, hot ionized component of the ISM. Vigorous star-forming regions may generate supergiant shells that blow out of galaxy disks, thereby dispersing metals and mass far from the parent star formation event. In addition, this mechanical energy contributes to ISM kinematics and is thought to be a primary source of turbulence (e.g., Norman & Ferrara 1996; Goldman 2000).

The effects of mechanical feedback have been clearly demonstrated, for example, in starburst galaxies (Johnson et al. 2000; Strickland et al. 2000) and in superbubbles around OB associations (e.g., Saken et al. 1992; Oey 1996). However, several troubling discrepancies remain unsolved. For example, almost all clean examples of bubbles blown by Wolf-Rayet stars and of superbubbles present shells that are too small for their observed parent stellar population (e.g., Treffers & Chu 1982; Drissen et al. 1995). Many superbubbles also show anomalous kinematics and X-ray emission (e.g., Rosado et al. 1982; Chu & Mac Low 1990; Wang & Helfand 1991). To resolve these puzzles and more clearly understand the mechanical feedback process, it is therefore necessary to examine simpler systems.

In active star-forming regions, high concentrations of OB stars collectively produce superbubbles. But in their peripheries, where stars are loosely distributed, discrete bubbles may be produced by individual stars. Hα images of H II regions ionized by OB associations in the Large Magellanic Cloud (LMC) have revealed large (50–150 pc) gas shells around the OB associations and numerous small (<15 pc) ringlike nebulae outside the large shell (see, e.g., Davies, Elliott, & Meaburn 1976). These small nebulae are candidate windblown bubbles of single O or B stars (Weis & Duschl 1999) and offer perhaps the simplest test of the standard adiabatic bubble model.

We have investigated the kinematics and physical nature of three ringlike nebulae in N44 (Henize 1956) in the LMC. N44 is a bright H II complex with a 44 pc × 67 pc superbubble at the center and several compact H II regions along the shell rim. In the surrounding area, small dense H II regions, as well as extended diffuse nebulae, are also present at distances up to 160 pc. Figure 1 shows these features and their identifications given by Henize (1956). Three OB associations exist in N44 (Lucke & Hodge 1970): LH 47 in the central shell, LH 48 in the compact H II region N44 I, and LH 49 partially embedded in the bright H II region N44 D. The three nebulae that we have studied are N44 F, N44 J, and N44 M. N44 F is a bright circular H II region at the northwest rim of the superbubble and is adjacent to a bright

[1] Institut d'Astrophysique et de Géophysique, Université de Liege, Allée du 6 Août 17, Bat. B5c, B 4000 Liège (Sart-Tilman), Belgium; naze@astro.ulg.ac.be.

[2] Research Fellow F.N.R.S. (Belgium).

[3] Department of Astronomy, University of Illinois, 1002 West Green Street, Urbana, IL 61801; chu@astro.uiuc.edu, mar@astro.uiuc.edu, gruendl@astro.uiuc.edu.

[4] Visiting astronomer, Cerro Tololo Inter-American Observatory.

[5] Lowell Observatory, 1400 West Mars Hill Road, Flagstaff, AZ 86001; oey@lowell.edu.

[6] Cerro Tololo Inter-American Observatory, Casilla 603, La Serena, Chile; csmith@noao.edu.

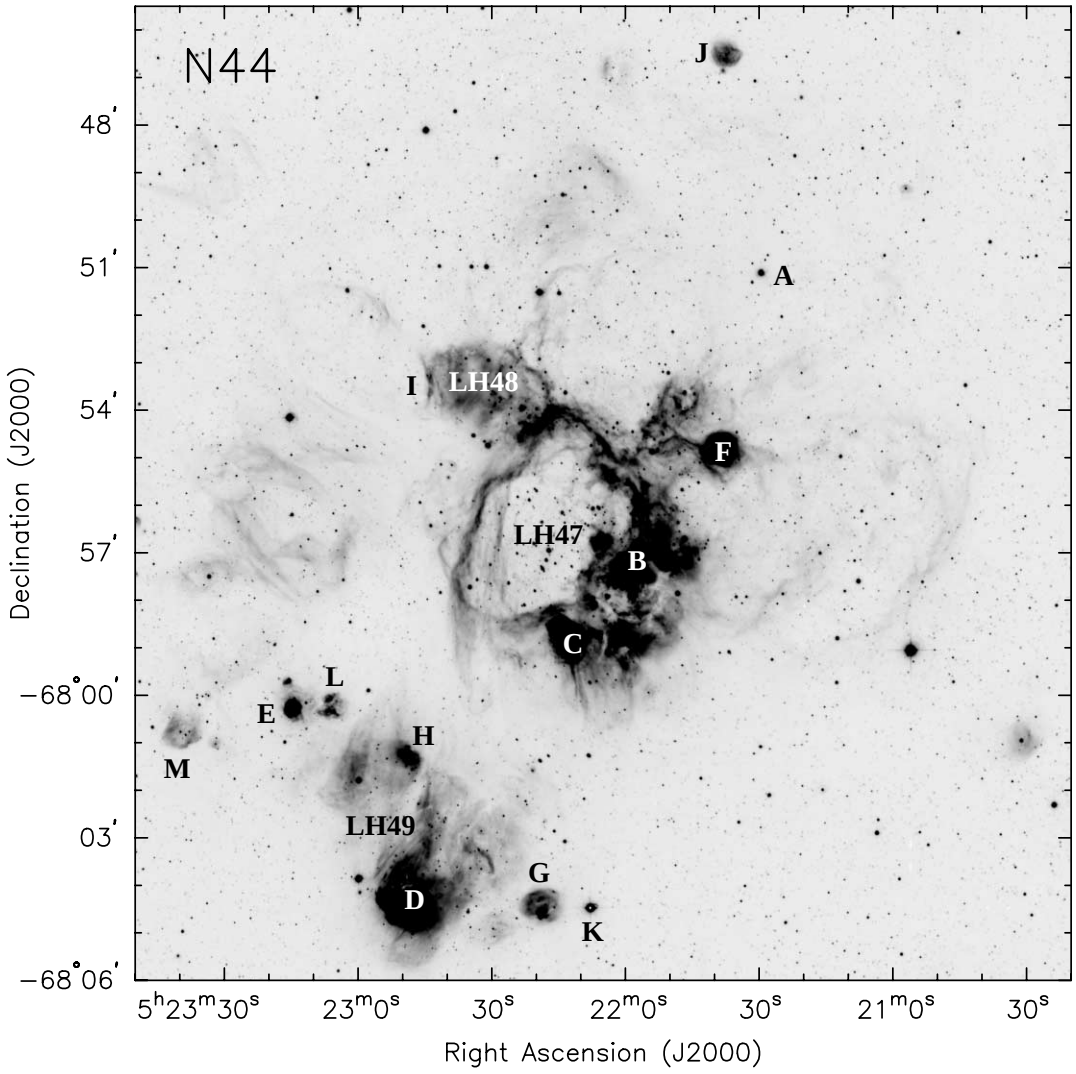

FIG. 1.—CTIO 0.9 m Hα (plus [N II]) CCD image of N44, showing the nebular components defined by Henize (1956) and the OB associations cataloged by Lucke & Hodge (1970).

filament connected to the main nebula. In contrast, N44 J and N44 M, appearing, respectively, on the northern and eastern parts of N44, are fainter and relatively isolated. None of these three nebulae have been studied since their original identification by Henize (1956).

We have obtained ground-based CCD images and high-dispersion echelle spectra of N44 F, N44 J, and N44 M to study the morphology and kinematics of these nebulae. Additionally, we have used *Hubble Space Telescope* (*HST*) Wide Field Planetary Camera 2 (WFPC2) images of N44 F in the Hα and [S II] lines to analyze its ionization structure. In this paper, we first describe these observations in § 2, then present the analysis and results for N44 F in § 3 and those for N44 J and N44 M in § 4. We present our conclusions in § 5.

2. OBSERVATIONS

The data sets used in this study include (1) CCD images taken with the Curtis Schmidt and 0.9 m telescopes at Cerro Tololo Inter-American Observatory (CTIO), (2) CCD images taken with the *HST* WFPC2, and (3) high-dispersion echelle spectra taken with the CTIO 4 m telescope. The high-dispersion spectra are useful to diagnose expanding shells that are not morphologically identifiable.

2.1. *Ground-based CCD Images*

CCD images of N44 were taken with the Curtis Schmidt telescope at CTIO in 1993 December. The detector was a front-illuminated Thomson 1024 × 1028 CCD camera with 19 μm pixels, or 1.″835 pixel^{-1}. Images were obtained with Hα ($\lambda_c = 6561$ Å, $\Delta\lambda = 26$ Å), [O III] ($\lambda_c = 5010$ Å, $\Delta\lambda = 50$ Å), and [S II] ($\lambda_c = 6720$ Å, $\Delta\lambda = 50$ Å) filters for exposure times of 1800, 2700, and 2700 s, respectively. The Hα filter includes not only the Hα line but also the neighboring [N II] $\lambda\lambda$6548, 6583 lines. At the LMC's radial velocity, $\sim$300 km s^{-1}, the [N II] λ6583 line is redshifted further away from the red edge of the filter, but the [N II] λ6548 line is redshifted further into the Hα bandpass. Using the [N II]/Hα intensity ratio measured from our echelle spectra (see § 2.3), we estimate that the [N II] λ6548 line emission contributes 2.4%, 4.3%, and 3.3% of the total flux of N44 F, N44 J, and N44 M, respectively. This [N II] contamination has been corrected in our Hα flux measurements.

Higher resolution Hα images were taken with the 0.9 m telescope at CTIO in 2000 December. The detector was a thinned AR-coated SITe 2048 $\times$ 2048 CCD with 24 μm pixels, or 0.″4 pixel^{-1}. The Hα filter ($\lambda_c = 6559$ Å, $\Delta\lambda = 64$ Å) used transmits Hα and both [N II] lines; therefore the "Hα" images are really Hα plus [N II] images and thus are used only for morphological analysis. The angular resolution, determined by the FWHM of the stellar images in the field of view, was approximately 1.″3. To map the entire N44 complex, five fields were observed with exposure times of 2 $\times$ 600 s for each field.

All CCD images were bias-subtracted and flat-fielded in a standard way using IRAF software, and multiple frames were combined to remove cosmic rays and improve the signal-to-noise ratio. Figure 1 shows the Hα mosaic of the N44 complex, and Fig. 2 presents close-ups of N44 F, N44 J, and N44 M in the Hα, [O III], and [S II] lines.

2.2. *HST WFPC2 Images*

HST WFPC2 images of N44 F were acquired via the Hubble Observation Problem Report[7] (HOPR) observations of Cycle 6 program 6698. In these observations, made

[7] The original observations of N44 were made with an incorrect orientation, resulting in a loss of $\frac{1}{3}$ of the field of view. To compensate for the loss, HOPR observations were granted. To facilitate the scheduling of these HOPR observations and to maximize the scientific yield, a different pointing center in N44 suitable for arbitrary orientations was chosen.

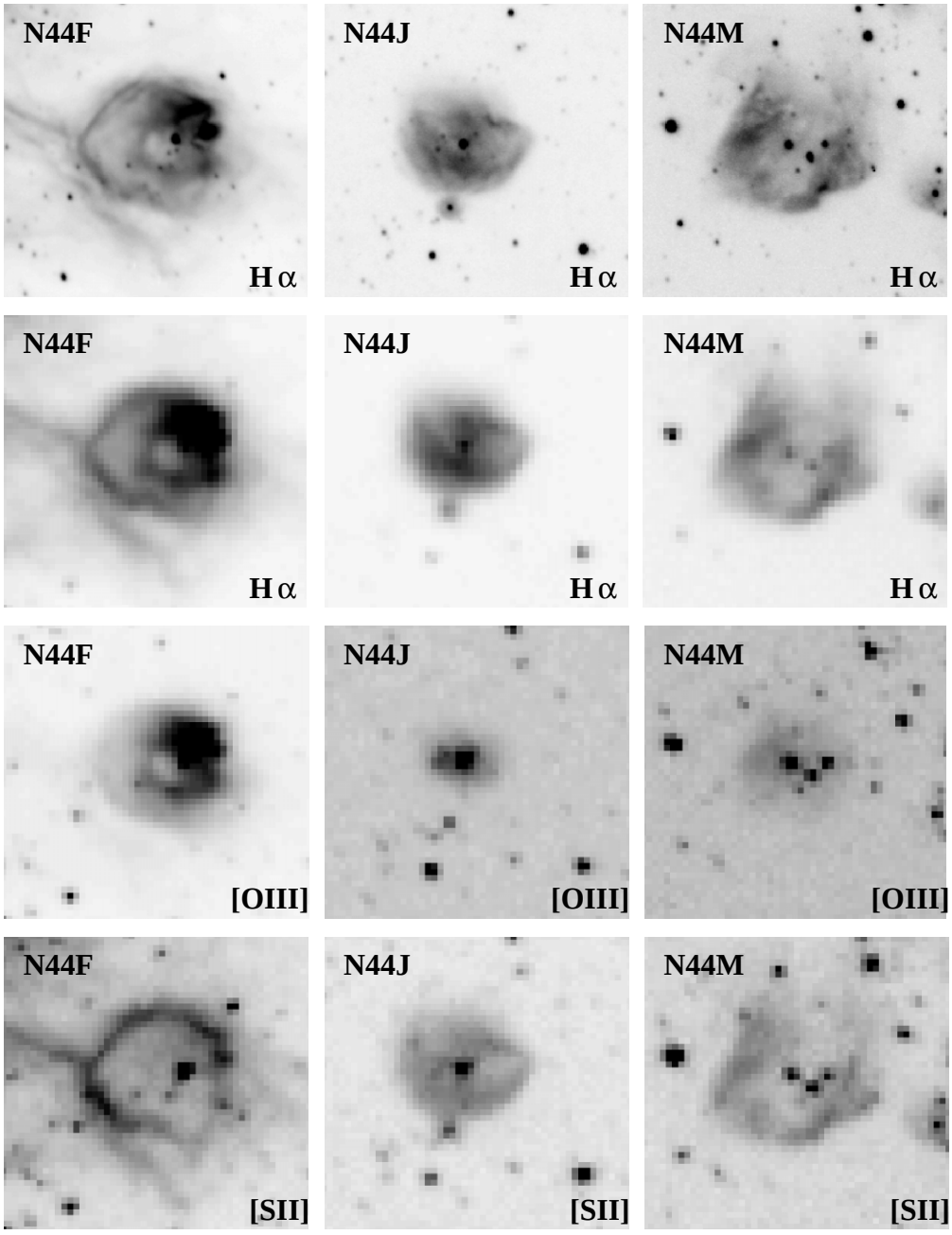

FIG. 2.—Ground-based images of N44 F (*left column*), N44 J (*middle column*), and N44 M (*right column*). The first row contains Hα (plus [N II]) images taken with the CTIO 0.9 m telescope. The second, third, and fourth rows contain Curtis Schmidt images taken in Hα (plus [N II]), [O III], and [S II] filters, respectively. The field of view (FOV) of each image is 92″ $\times$ 92″. North is up, and east to the left.

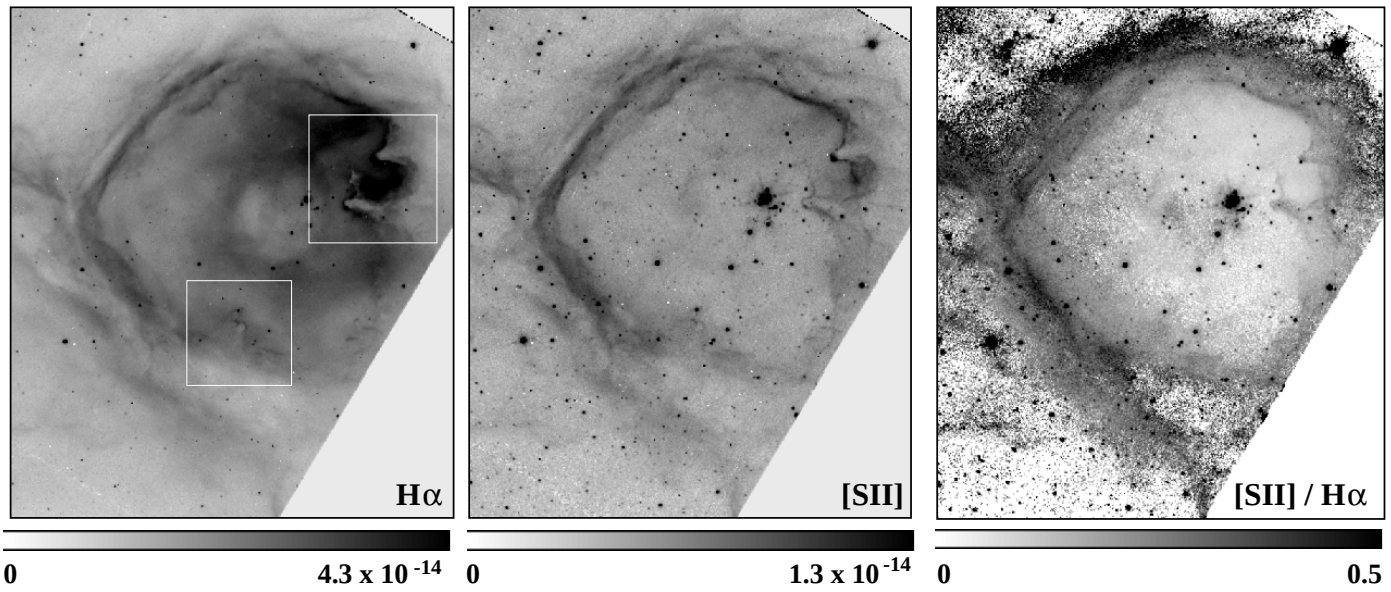

FIG. 3.—*HST* WFPC2 Hα (plus [N II]) image (*left*), [S II] image (*middle*) and [S II]/Hα ratio map (*right*) of N44 F. The rectangular boxes show the position of the close-up images presented in Fig. 4. The bars below the images show the gray scales for surface brightness (in units of ergs cm^{-2} s^{-1} $arcsec^{-2}$) or line ratio. North is up, and east to the left.

with the F656N filter for 2 × 500 s and the F673N filter for 2 × 600 s, N44 F was included in the Wide-Field Camera 3. The F656N filter, centered at 6563.7 Å with an FWHM of 21.4 Å, includes the Hα line and the neighboring [N II] lines. Using the [N II]/Hα intensity ratio measured from our echelle spectra (see § 2.3), we estimate that the [N II] λ6548 line emission contributes 2.4% of the flux in N44 F. This [N II] contamination has been corrected in our Hα flux measurements. The F673N filter, centered at 6732.2 Å with an FWHM of 47.2 Å includes the nebular lines of [S II] λλ6716, 6731.

The calibrated WFPC2 images were produced by the standard *HST* pipeline. We processed them further with IRAF and STSDAS routines. The images taken with the same filter were combined to remove cosmic rays and to produce a total exposure map. The combined [S II] and Hα images were then each corrected for the intensity- and position-dependent charge transfer efficiency as explained by Holtzman et al. (1995). Following the recommended procedures for narrowband WFPC2 photometry,[8] we find the rectangular widths of the F656N and F673N filters to be 28.3 and 63.3 Å, respectively, and use these widths to convert the flux densities into fluxes.

Figure 3 shows the WFPC2 images of N44 F. To show the excitation variations, the [S II]/Hα ratio map of N44 F is also presented, in addition to the Hα and [S II] images.

2.3. *CTIO 4 m Echelle Spectra*

Echelle spectra were obtained with the CTIO 4 m telescope in 2000 December. The spectrograph was used with a 79 line mm^{-1} echelle grating and the long-focus red camera. We observed a single order centered on the Hα line by inserting a postslit Hα interference filter and replacing the cross-dispersing grating with a flat mirror. A Tektronix 2048 × 2048 CCD with 24 μm $pixel^{-1}$ was used to record the images. This provided a spectral sampling of ∼0.08 Å $pixel^{-1}$ and a spatial sampling of 0.″26 $pixel^{-1}$. The wavelength coverage, limited by the Hα filter and the echelle order, was 125 Å; the spatial coverage, limited by the optics, was ∼200″. The angular resolution, determined by the FWHM of the seeing, was approximately 1″. A slit width of 1.″65 was used. The resultant spectral resolution, measured from the ThAr lamp lines, was about 13 km s^{-1} FWHM.

Each of the three nebulae, N44 F, N44 J, and N44 M, was observed with an east-west oriented slit. The exposure times were 600 s for N44 F, but only 300 s for N44 J and N44 M. The spectral lines detected include nebular Hα and [N II] lines and telluric Hα and OH lines (Osterbrock et al. 1996). We have adopted rest wavelengths of 6562.7885, 6548.080, and 6583.454 Å for the Hα and [N II] λλ6548, 6583 nebular lines, respectively (Spyromilio 1995).

3. PHYSICAL STRUCTURE OF N44 F

We will first describe the overall morphology of N44 F, examine its excitation and ionization structure, and derive its rms electron density. Special emphasis is given to the prominent dust "pillars," where star formation might be taking place. Next, we describe the kinematic features detected in the echelle spectra, fit Gaussian components to the line profiles, and use the resultant velocities to identify expanding structures and to determine expansion velocities. Finally, we combine the morphological and kinematic information and present an integrated view of this H II region. Throughout this paper, we will adopt a distance of 50 kpc to the LMC (Feast 1999).

3.1. *Morphology and Density*

N44 F is a bright circular nebula nestled on a bright filament at the northwest rim of the superbubble in N44. In low-resolution Hα images, N44 F appears to have a double-ring structure with a very bright region in the northwest.

[8] Available at http://www.stsci.edu/instruments/wfpc2/Wfpc2_faq/wfpc2_nrw_phot_faq.html.

The details of these features are resolved in the *HST* WFPC2 images. The outer ring, of radius $\sim 22''$, is surrounded by dusty features. Finger- or pillar-like dust columns, similar to those in the Eagle Nebula (=M16; Hester et al. 1996), are also seen at the periphery, with two especially prominent ones at the west, close to the brightest region of N44 F. These dust columns are revealed in detail by the *HST* images and will be discussed more extensively in § 3.2. The inner ring, of radius $\sim 6''$, is resolved into diffuse emission without sharp features. The western part of this ring merges into the brightest region of N44 F. A group of bright stars are located within the central ring, but they are substantially offset toward the bright emission region at the northwest. Unfortunately, none of the stars in the vicinity of N44 F have been studied photometrically or spectroscopically.

The [S II] images of N44 F show a very different morphology: only the outer ring is visible and it is mostly composed of sharp filaments. The pillar-like features are also present and stars at the tips of two of them are clearly seen (see Fig. 4). The [S II]/Hα ratio in the central region is very low, about 0.1. The outer ring possesses a higher [S II]/Hα ratio, with values ranging from 0.2 to 0.4. Enhanced [S II]/Hα ratios are often associated with shell structures or high-

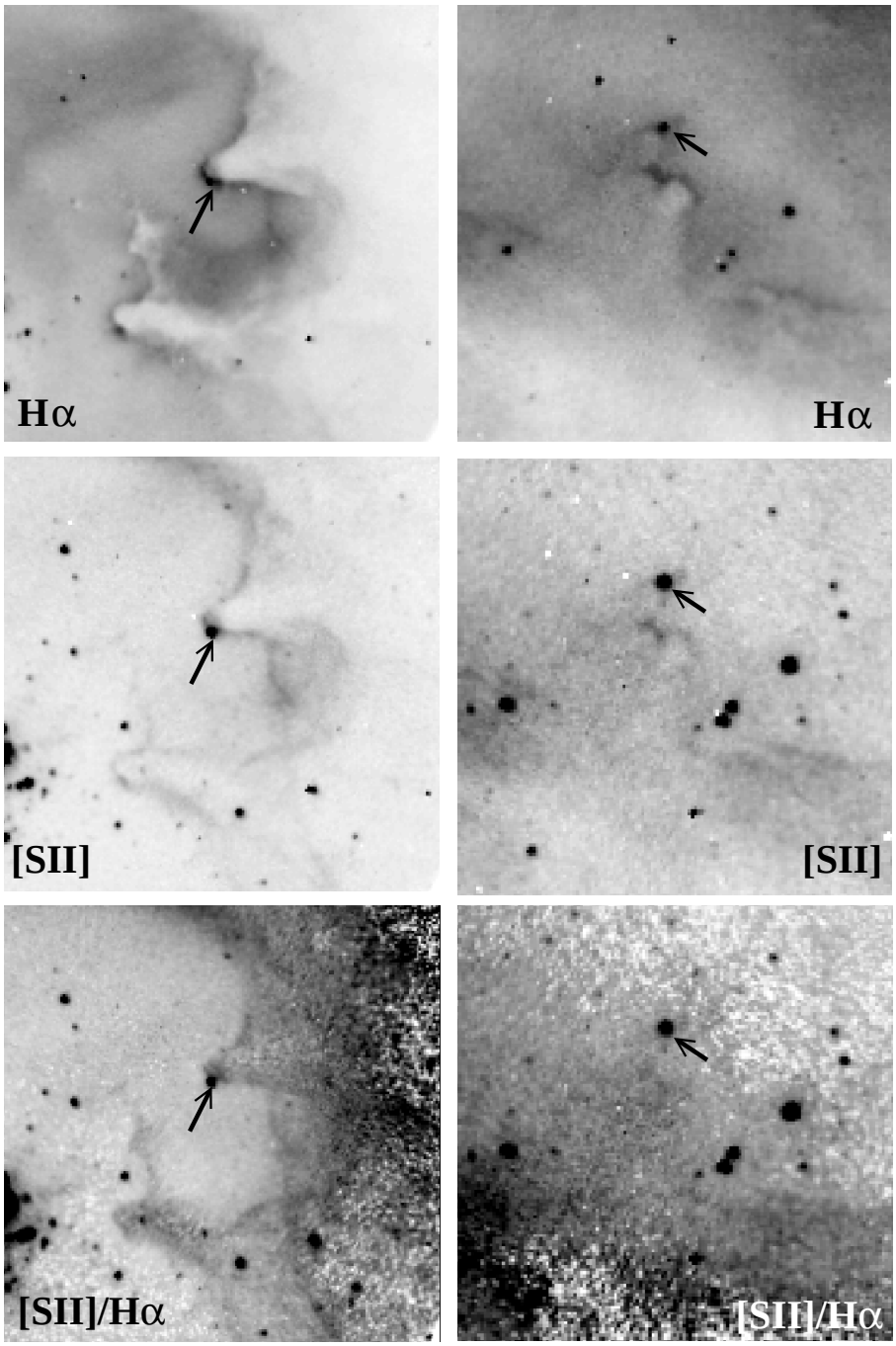

FIG. 4.—Close-up images of dust columns seen in N44 F through Hα, [S II], and [S II]/Hα (for exact position, see Fig. 3). *Left*, Dust columns situated at the west rim of N44 F (FOV = $18'' \times 18''$); *right*, dust columns situated at the south rim of N44 F (FOV = $14'' \times 14''$). The arrows point to the stars at the tips of the pillar-like dust columns.

velocity shocks. As we do not find the latter in the nebula (see § 3.3), the somewhat elevated [S II]/Hα ratio is likely to result from the low-ionization parameter[9] caused by the shell morphology. The values of [S II]/Hα are in fact similar to those seen in other shell structures (e.g., Lasker 1977; Hunter 1994).

Using the Curtis Schmidt images, we also examine the [O III] morphology of N44 F. Because of the poorer resolution, only the overall morphology can be described. The [O III] image of N44 F looks very similar to that in Hα, except for the bright Hα outer ring, which disappears almost completely in [O III]. We have used the *HST* WFPC2 observations of N44 C (Garnett, Galarza, & Chu 2000) to calibrate the observed [O III]/Hα ratio derived with the Curtis Schmidt images. The [O III]/Hα ratio of N44 F is relatively high, about 0.5–1.2 inside the ring, with the highest value near the star(s). The outer ring has the lowest [O III]/Hα ratio, about 0.25. The integrated [O III]/Hα ratio for the whole nebula is about 0.55. The high ratio near the central region indicates that the ionizing source must be an early-type massive star.

The WFPC2 Hα image can be further analyzed to estimate the rms density of N44 F. A color excess of $E(B-V) = 0.11$ mag for N44 (Oey & Massey 1995) is adopted in the extinction correction. The emission measure (EM) derived from the extinction-corrected surface brightness (Peimbert, Rayo, & Torres-Peimbert 1975) ranges from 7×10^3 cm^{-6} pc in the faintest interior regions of N44 F to 4×10^4 cm^{-6} pc at the tips of the "pillars." To derive the density from the EM, we can assume two simple geometries. First, the density can be estimated by assuming the depth to be equal to the diameter of the nebula: for the central region, we find a value ranging from 25 to 35 cm^{-3}. Second, N44 F is limb-brightened and we can therefore estimate the density by assuming a constant-density spherical shell with radius R and thickness ΔR. This geometry predicts a unique radial surface brightness profile for any $\Delta R/R$, based on the varying path length through the shell material. Comparing these simple modeled profiles with the observed Hα surface brightness profiles near the shell rim, we find a shell thickness $\Delta R/R$ of $\sim$0.25. Using the peak surface brightness and the length of the longest line of sight,

$$2\sqrt{2R\Delta R - (\Delta R)^2}\,,$$

we then derived a density in the shell of 40 cm^{-3}. On average, the diffuse gas of N44 F probably possesses a density of a few tens cm^{-3}.

Using the Curtis Schmidt Hα image and the flux calibration from Kennicutt & Hodge (1986), we measured over the entire N44 F nebula an Hα flux of 3.6×10^{-11} ergs cm^{-2} s^{-1}. For a distance of 50 kpc, the Hα luminosity of N44 F is then 1.4×10^{37} ergs s^{-1}, after correcting for an extinction of $E(B-V) = 0.11$ mag. This Hα luminosity requires an ionizing flux of $Q(H^0) = 1.0 \times 10^{49}$ photons s^{-1}. A second evaluation of the extinction correction has been made by comparing radio data and the Curtis Schmidt Hα image: a mean value $E(B-V)$ of 0.28 mag for N44 F, N44 J, and N44 M is found (J. R. Dickel 2002, private communication), and this results in a $Q(H^0)$ of 1.4×10^{49} photons s^{-1} for N44 F. This value suggests that the total ionizing power of the star(s) within N44 F is equivalent to a single O6.5 V–O7.5 V star (Panagia 1973; Vacca, Garmany, & Shull 1996; Schaerer & de Koter 1997). This is compatible with the rather high [O III]/Hα ratio: the photoionization models of Stasińska & Schaerer (1997) for CoStar stellar atmosphere models suggest that the observed integrated [O III]/Hα ratio of N44 F could be produced by the equivalent of an O8 V–O9 V star.[10] The comparison with the photoionization models should however be interpreted with caution because the models do not assume a shell structure, which affects the excitation and ionization structure. The dominant spectral type could therefore be somewhat earlier than inferred from the modeled excitation.

3.2. *Pillar-like Dust Columns*

The dark clouds of N44 F exhibit new examples of the intriguing finger- or pillar-like structures, similar to those reported in the Eagle Nebula (Hester et al. 1996). The most prominent two are embedded in the bright northwest region (see Figs. 3 and 4). Several additional features of this type are present in the south and possibly in the southwest, but they are fainter. In Figure 4, we present the most striking of these structures in the Hα and [S II] images, as well as in the ratio map. The dust columns in N44 F are 5″ to 10″ long and 1″ to 2 ″ wide, corresponding to 1 to 2 pc long and 0.25 to 0.5 pc wide at the LMC's distance. These sizes and morphologies are similar to those seen in 30 Doradus (Scowen et al. 1998) and M16 (Hester et al. 1996). Two of these columns harbor stars at their tips, as indicated by arrows in Figure 4. Hester et al. (1996) suggested that stars at the tips of pillars could be young stellar objects that were formed in the molecular cloud and finally emerge after the photoevaporation of most of their parent cloud. However, the Hester et al. (1996) model of preexisting condensations in the molecular cloud does not provide the unique conditions for producing photoionized pillars. Hydrodynamical simulations by Williams, Ward-Thompson, & Whitworth (2001) illustrate that these structures can be formed by a variety of initial conditions in the structure with inhomogeneities in density and/or radiation field, but current observations do not yet permit discrimination among these different models. It is therefore of great interest to identify additional examples of such objects.

Other important characteristics of these dust columns are their ionization structure and their density. All the dust columns point toward the central ionizing source, i.e., a bright star or a small cluster between the center and the northwest edge of N44 F.

As can be seen in Figure 5, the [S II] peak is separated from the Hα peak by approximately 0.″1, i.e., 0.024 pc, with Hα peaking slightly closer to the source of UV radiation that is photoevaporating the cloud. The shape of these profiles is very similar to those observed in the pillars of 30 Doradus or in ground-based images of M16 (Scowen et al.

[9] The ionizing flux derived further can be used to estimate the ionization parameter $U \propto [Q(H^0)nf^2]^{1/3}$, where $Q(H^0)$ is the ionizing flux in photons per second, n the density in cm^{-3}, and f the filling factor. Using $Q(H^0) = 1.0 \times 10^{49}$ photons s^{-1}, $n = 40$ cm^{-3} and $f = 1 - [1 - (\Delta R/R)^3] \sim 0.6$, we find a value of $\sim 10^{-3}$ for the ionization parameter.

[10] We have compared N44 F, N44 J, and N44 M to the closest model available in Stasińska & Schaerer (1997), i.e., a spherical nebula of density 10 cm^{-3} and metallicity 0.25 $Z_\odot$, ionized by one single star.

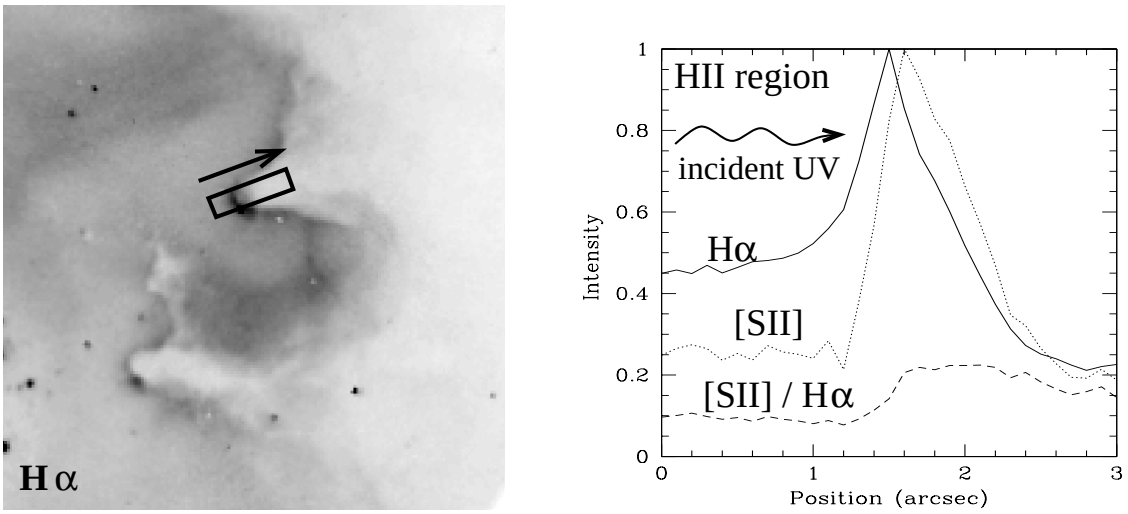

FIG. 5.—*Left*: Hα image of the "pillars" situated at the west part of N44 F. The rectangular box and the arrow show the position and direction of the cut presented at the right. *Right*: Ionization structure along the rectangular aperture. [S II] and Hα intensities are normalized to the peak, while the [S II]/Hα ratio is the actual value. Note that the Hα and [S II] peaks are separated by 1 pixel, i.e., 0.″1.

1998). Unfortunately, no WFPC2 [O III] images of N44 F are available; thus we cannot undertake a complete analysis using photoionization models or constrain further the properties of the ionizing source. Following the method used in § 3.1, we estimate an rms density larger than 300 cm^{-3} at the tip of one of the pillars. This density is compatible with that determined by Scowen et al. (1998) in 30 Doradus, 700 cm^{-3}. These pillars are thus photoevaporating clouds, whose evaporated matter enhances the density and brightness of the diffuse material seen in the northwest part of the nebula.

3.3. *Kinematic Properties*

The kinematic properties of N44 F are derived from the high-dispersion echelle observations of the Hα and [N II] λ6583 lines. The [N II] line has a smaller thermal width than the Hα line; thus it shows the line splitting better although it is noisier. We have extracted Hα and [N II] line profiles and fitted them with Gaussian components. The resultant velocity-position plot (Fig. 6) shows that N44 F is an expanding shell with a radius of 22″, coincident with the outer ring described in § 3.1. Both lines indicate a shell expansion velocity of $\sim$12 km s^{-1}. An example of the [N II] and Hα profiles are presented in Figure 7. The approaching (blue-shifted) component is fainter, suggesting a lower density. Farther east, outside N44 F, an additional blue component is present, but it is probably associated with the complex filamentary structure at the outskirts of N44 and is not directly related to N44 F.

3.4. *Test of the Standard Bubble Model*

N44 F has a classical ring-nebula morphology, and its kinematics confirms an expanding shell, most likely created by the wind of the early-type massive star(s) within this bubble. We can now test whether the observed expansion dynamics of this bubble are consistent with those expected from the standard adiabatic bubble model (e.g., Weaver et al. 1977). With the observed radius R in parsecs and the expansion velocity V in kilometers per second, we can compute the dynamical timescale t_6 in units of 10^6 yr by using $t_6 = 0.6R/V$ and further determine the ratio of stellar wind luminosity L_{36} in units of 10^{36} ergs s^{-1} to ambient density n_0 in units of H atoms cm^{-3}, using

$$R = 27\left(\frac{L_{36}}{n_0}\right)^{1/5} t_6^{3/5} .$$

For a radius of 5.3 pc and an expansion velocity of $\sim$12 km s^{-1}, N44 F has a dynamical timescale of 2.7×10^5 yr and a L_{36}/n_0 ratio of 0.016 ergs s^{-1} cm^3. If we assume that the shell consists of mass swept up from the volume, the ambient density, n_0, can be estimated by $n_0 = 3n(\Delta R/R)$, where n is the rms density of the shell, ΔR the shell thickness, and R the shell radius. For $n \sim 40$ cm^{-3} and $\Delta R/R = 0.25$ (see § 3.1), we derive an ambient density of $\sim$30 cm^{-3} and a wind luminosity of $\sim 5 \times 10^{35}$ ergs s^{-1}. This wind luminosity is compatible with that expected from the spectral type determined in § 3.1, i.e., an O7 V star (de Jager, Nieuwenhuijzen, & van der Hucht 1988; Prinja, Barlow, & Howarth 1990). One uncertainty in these estimates is the shell thickness; however, even if the shell thickness is off by a factor of 2, the predicted wind luminosity will still be compatible, within the errors, with an O7 V star.

Thus, the dynamics of N44 F appear to be consistent with the standard adiabatic model for bubble evolution, within uncertainties generated by the complex interstellar environment. This contrasts with the results from superbubbles, which show evidence of retarded growth (e.g., Oey 1996). To investigate this discrepancy further, it is worth considering an alternative bubble model.

The presence of dust pillars around N44 F clearly indicates a highly inhomogeneous ISM. The photoevaporation of the dense clumps may serve as an energy sink and govern the dynamic evolution of this H II region. Since photoevaporation processes take place in the early evolutionary stages of a bubble or superbubble, the energy loss by photoevaporation may explain the smaller-than-expected sizes of previously studied superbubbles and Wolf-Rayet ring nebulae (see § 1). Therefore, we will now consider models of bubbles

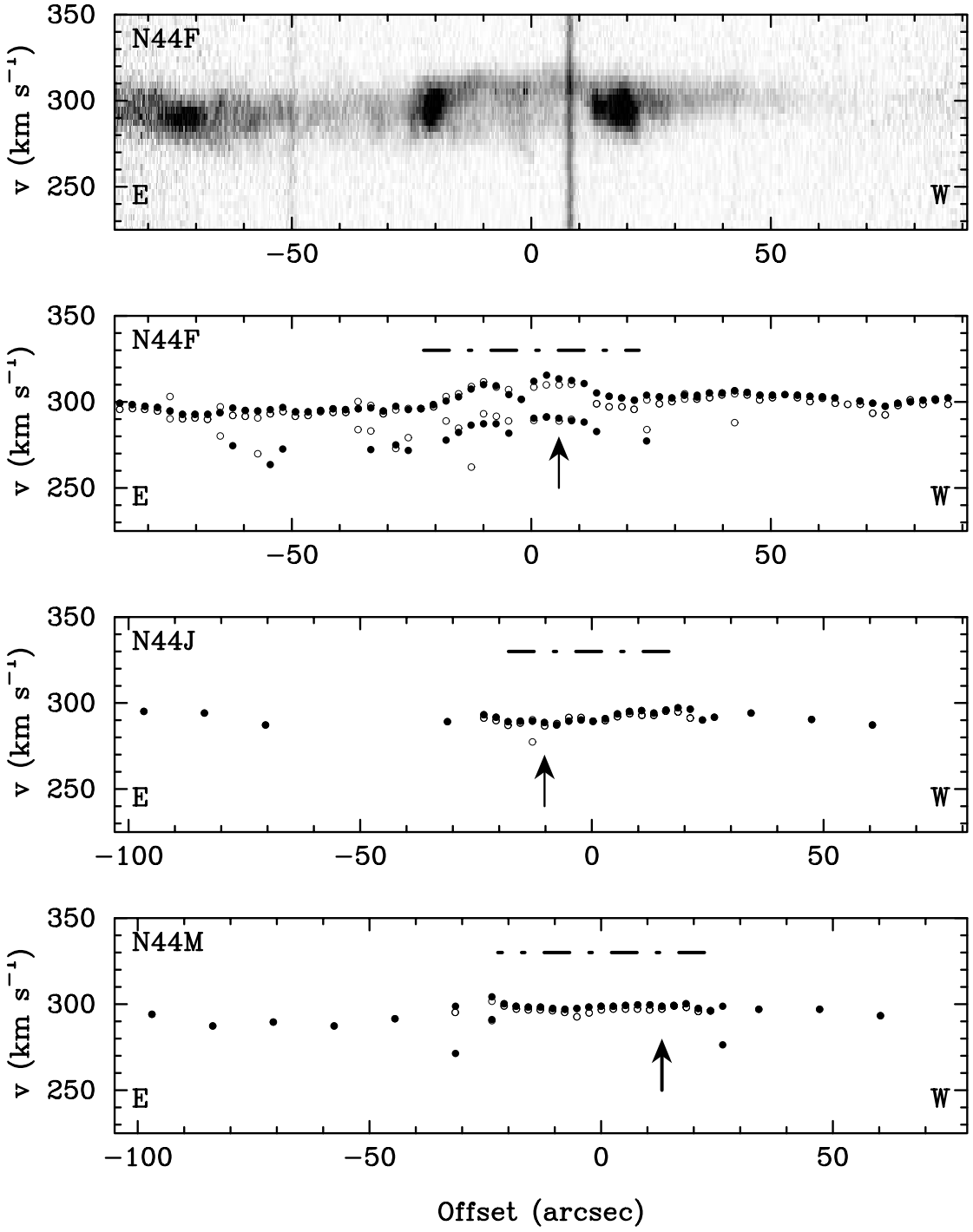

FIG. 6.—*Top*, Echellogram of the [N II] λ6583 line for N44 F; *lower*, radial velocity-position plots of the echelle slit positions in N44 F, N44 J, and N44 M for both Hα and [N II] lines. The radial velocities are heliocentric. The Hα velocity components are plotted in filled circles, and the [N II] in open circles. The position axis is defined with the center of the nebula at the origin (0″) and increasing toward the west. The dot-dashed line in each plot indicates the range covered by the nebula. Arrows show the positions of the profiles presented in Fig. 7.

formed in a cloudy medium by McKee, Van Buren, & Lazareff (1984). In their models, only bubbles blown by stars with weak winds will follow the Weaver et al. model, while stars with stronger winds will produce bubbles whose expansion is governed by the dynamics of photoevaporating clouds. They define a dimensionless wind luminosity

$$L_W^* \equiv L_W / \left[1.26 \times 10^{36} (S_{49}^2 / n_m)^{1/3}\right]$$

and a homogenization radius

$$R_h(\mathrm{pc}) \equiv 0.009 t^{4/7} \left(\frac{S_{49}}{n_m^2}\right)^{1/7},$$

where L_W is the wind luminosity in ergs s^{-1}, S_{49} the ionizing flux in photons s^{-1}, n_m the mean cloud density in cm^{-3} and t the dynamical timescale in years. Strong winds possess $L_W^* \gtrsim 1$ and blow bubbles of radius $\sim R_h$.

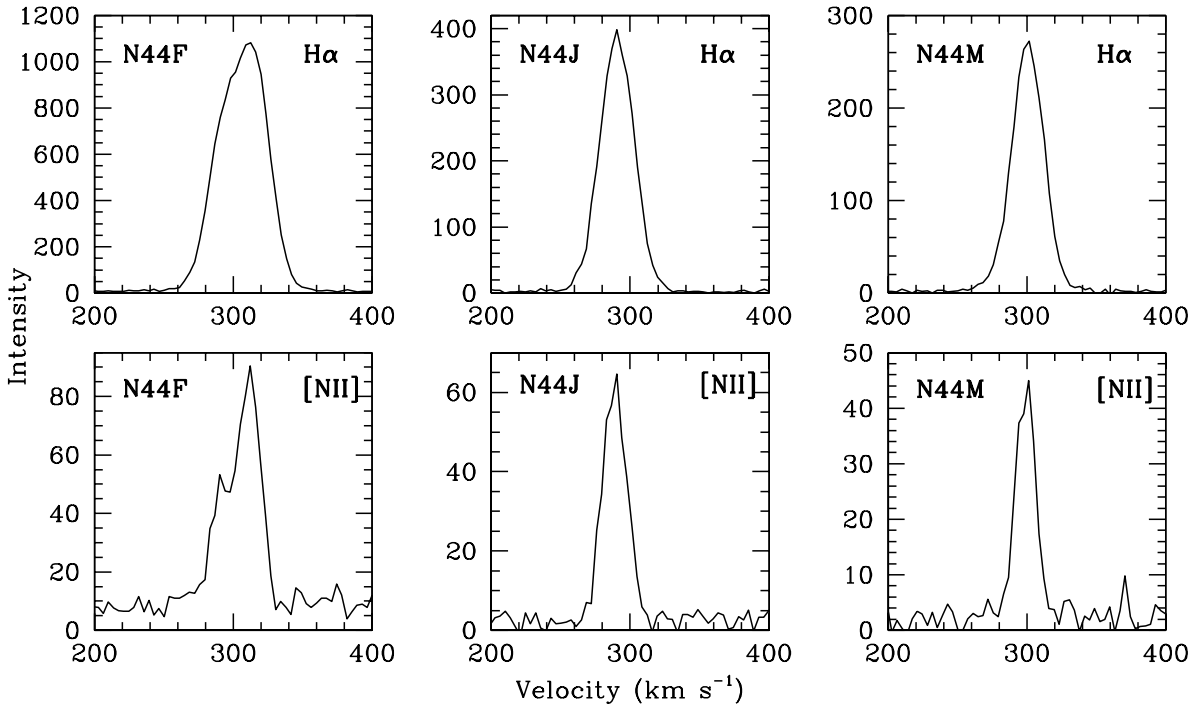

FIG. 7.—Hα and [N II] profiles at the positions indicated in Fig. 6

Using the observed parameters of N44 F (with $n_m = n_0$) and assuming a stellar wind luminosity for an O7 V star, we estimate $L_W^* \sim 1$ and $R_h \sim 4.5$ pc, close to the observed bubble's radius. This seems to suggest that the dynamics of photoevaporation actually governs the bubble's expansion. The agreement of the data with both models could be a simple coincidence, or maybe the bubble has just encountered the cloudy medium and begun the photoevaporation processes, in which case there may not be a large deviation from the Weaver et al. model. Note, however, that all these conclusions hinge upon the validity of the stellar wind luminosity, which is based on an assumed spectral type of the central star. Future study of the actual stellar content of N44 F is needed to place stronger constraints on the applicable bubble models.

4. PHYSICAL STRUCTURE OF N44 J AND N44 M

4.1. *N44 J*

Situated in the northernmost part of the N44 complex, N44 J is a slightly elongated, ringlike nebula of size $37'' \times 32''$(or 9.0 pc $\times$ 7.8 pc). The 0.9 m Hα image shows a bright rim around dusty features at the northwest boundary. A bright central star is visible in the Hα and [S II] images (see Fig. 2). In Hα and [S II], the nebula exhibits modest limb-brightening, with the edge-to-center brightness ratio less than 2, while its central part displays a rather uniform surface brightness. The [S II]/Hα ratio is very similar to that of N44 F, ranging from 0.25 to 0.4. In contrast, the [O III] image of N44 J shows emission only near the central star. The [O III]/Hα ratio is 0.4 near the star, and only 0.05–0.08 elsewhere, significantly lower than the corresponding value in N44 F. The integrated [O III]/Hα ratio of N44 J is about 0.12.

The observed Hα flux of N44 J is 5.7×10^{-12} ergs cm^{-2} s^{-1}. This requires an ionizing flux $Q(H^0)$ of 1.6×10^{48} photons s^{-1} when adopting $E(B-V) = 0.11$ mag, or 2.3×10^{48} photons s^{-1} for $E(B-V) = 0.28$ mag. These values are expected for an O9 V–B0 V type ionizing star (Panagia 1973; Vacca et al. 1996; Schaerer & de Koter 1997), which is fully consistent with that suggested by the [O III]/Hα ratio of the nebula (Stasińska & Schaerer 1997). Assuming a spherical geometry, we derive an rms electron density of $\sim$25 cm^{-3}, slightly less dense than N44 F. The ionized gas mass of N44 J is then $\sim$200 $M_\odot$.

The echelle spectrum of N44 J shows a kinematically quiescent H II region. The centroids of the Hα and [N II] lines are centered at 292 km s^{-1}, with an rms variation of 3 km s^{-1} (see Figs. 6 and 7). No line splitting is seen. The observed FWHMs are 27 ± 1 km s^{-1} for Hα and 16 ± 2 km s^{-1} for [N II]. These observed line widths imply a turbulent FWHM of about 10 km s^{-1} for Hα and 8 km s^{-1} for [N II] if we take into account the instrumental profile and the thermal broadening at 10^4 K. The turbulence can thus explain the small variations of the centroid velocity. The difference between the turbulence widths is probably caused by a difference in the emission regions of the two lines. If N44 J is actually expanding, the expansion velocity should be very small, less than 8 km s^{-1}. For such small expansion velocity, no strong compression is expected, hence no sharp filaments should be seen.

Finally, we may compare the observations with the standard adiabatic bubble model. As the density in the ringlike nebula is a few tens cm^{-3}, we will assume in our calculations a density of 10 cm^{-3} in the ISM. For an expected wind luminosity of $\sim 3 \times 10^{34}$ ergs s^{-1} for an O9.5 V star (de Jager et al. 1988; Prinja et al. 1990) and with the observed 17.″5 radius of N44 J, the Weaver et al. (1977) model predicts an expansion velocity of about 8 km s^{-1} for N44 J. This

expected expansion velocity is just at the limit implied by the velocity widths of the Hα and [N II] lines. Raising the ambient density by a factor of 2 can lower the expected expansion velocity to 6.5 km s^{-1}, which is more consistent with the observed limit. We conclude that the observed bubble dynamics of N44 J does not greatly contradict the model predictions.

4.2. *N44 M*

On the southeast part of N44, another small ringlike nebula is present: N44 M. It is the faintest nebula of our sample. It shows a ring with a radius of $\sim$22″ (or 5.3 pc), but its north boundary is not well defined (see Fig. 2). The sharp southwest boundary suggests the presence of dust clouds. Several bright stars appear in its interior. N44 M possesses an excitation structure very similar to N44 J. The [S II]/Hα ratio of N44 M is comparable to that in N44 F, but the [O III]/Hα ratio of N44 M is much lower, ranging from 0.07 to 0.16 in the nebula and rising to 0.4 near the stars. The integrated [O III]/Hα ratio of N44 M is about 0.18.

With an observed Hα flux of 5.3×10^{-12} ergs cm^{-2} s^{-1} and the two evaluations of the extinction, the required ionizing flux $Q(H^0)$ is (1.5–2.1)$\times$ 10^{48} photons s^{-1}. This suggests an O9–B0 V type ionizing star (Panagia 1973; Vacca et al. 1996; Schaerer & de Koter 1997), which is again compatible with the [O III]/Hα ratio (Stasińska & Schaerer 1997). If we assume a spherical geometry, we find that the rms density is about $\sim$17 cm^{-3} and the estimated mass of the nebula $\sim$275 $M_\odot$.

The echelle spectrum of N44 M shows only one component, centered at 298 km s^{-1} with an rms variation of 1 km s^{-1} and an FWHM of 28 $\pm$ 1 km s^{-1} in the Hα line and 20 $\pm$ 4 km s^{-1} in the [N II] line (see Figs. 6 and 7). The turbulent FWHMs are then 12 km s^{-1} for Hα and 14 km s^{-1} for [N II]. With an observed radius of $\sim$22″, a density of 10 cm^{-3} for the ISM, and a O9.5 V ionizing star (see § 4.1.), the standard bubble model predicts an expansion velocity of $\sim$7 km s^{-1} for N44 M, which appears consistent with the upper limit of the echelle observations.

The kinematic characteristics of N44 J and N44 M are very similar, despite the somewhat different morphology. Neither H II region contains shells expanding at velocities greater than $\sim$8 km s^{-1}. In the future, additional observations may enable a better comparison of these nebulae with the standard model. Precise photometry and/or stellar spectroscopy would give accurate information about the stellar content of these nebulae, while nebular spectra with higher resolution should more strongly constrain the kinematics of N44 J and N44 M. Thus, improved data are needed to more stringently test the standard model for N44 J and N44 M.

5. CONCLUSION

Massive stars inject a large amount of energy into the ISM through their ionizing radiation, fast stellar winds, and SNe. The stellar winds, which dominate the early mechanical feedback, are able to sweep the ambient medium into an expanding shell and create a cavity around the parent stars. H II regions ionized by massive stars are therefore thought to evolve from compact H II regions to ringlike nebulae.

We have studied three candidate windblown bubbles in the N44 complex: N44 F, N44 J, and N44 M. They all have diameters of $\sim$10 pc. Their ionizing fluxes and [O III]/Hα ratios suggest that their ionizing stars have spectral types of roughly O7 V, O9.5 V, and O9.5 V, respectively. N44 F has an expansion velocity of 12 km s^{-1}, while the other two have expansion velocities less than 8 km s^{-1}. The stellar wind luminosity implied by the ionizing stars and the observed bubble dynamics appear consistent with that expected in the standard adiabatic bubble model within the limits of observational uncertainties. Similar results were found by Oey & Massey (1994) for two bubbles around a single O star in M33. This is in sharp contrast to the anomalous kinematics seen in superbubbles and Wolf-Rayet bubbles. We caution, however, that our observed expansion velocities may not provide the most stringent constraints when comparing with models, because the expected expansion velocities of N44 J and N44 M are comparable to or smaller than the convolution of the isothermal sound velocity ($\sim$10 km s^{-1}) and the instrumental FWHM (13 km s^{-1}). Deeper, higher resolution spectroscopic observations of the [N II] or [O III] lines are needed to pin down the expansion velocity for a more definitive test of models.

We also report the discovery of several dust pillars in N44 F, which are similar to those found in the Eagle Nebula (Hester et al. 1996) and 30 Doradus (Scowen et al. 1998). These structures are indicative of the evaporation of molecular clouds by the ionizing source. The examples in N44 F are especially well-suited to investigating the process and role of photoevaporation in star formation and shell evolution, because of their location within such a well-defined, windblown bubble. We found that photoevaporation, as evidenced by the pillar structure, may be dynamically important for the shell evolution in N44 F, slowing down the expanding shell and inhibiting its growth. These photoevaporation processes may thus undermine the seeming agreement between the observed bubble dynamics and the simple adiabatic bubble model.

We thank Charles Danforth for assisting in the echelle observations and Rosie Chen for help in the *HST* WFPC2 image reduction. This work has been supported by the NASA grant STScIGO-6698.01-95A. Y. N. acknowledges support from the F.N.R.S., contracts P4/05 and P5/36 "Pôle d'Attraction Interuniversitaire" (SSTC-Belgium) and the PRODEX XMM-OM and Integral Projects. R. C. S. acknowledges the support of the Dean B. McLaughlin fellowship at the University of Michigan and NSF grant AST 95-30747.

REFERENCES

Chu, Y.-H., & Mac Low, M.-M. 1990, ApJ, 365, 510
Davies, R. D., Elliott, K. H., & Meaburn, J. 1976, MmRAS, 81, 89
de Jager, C., Nieuwenhuijzen, H., & van der Hucht, K. A. 1988, A&AS, 72, 259
Drissen, L., Moffat, A. F. J., Walborn, N. R., & Shara, M. R. 1995, AJ, 110, 2235
Feast, M. 1999, in IAU Symp. 190, New Views of the Magellanic Clouds, ed. Y.-H. Chu, N. Suntzeff, J. Hesser, & D. Bohlender (San Francisco: ASP), 542
Garnett, D. R., Galarza, V. C., & Chu, Y.-H. 2000, ApJ, 545, 251
Goldman, I. 2000, ApJ, 541, 701
Henize, K. G. 1956, ApJS, 2, 315
Hester J. J., et al. 1996, AJ, 111, 2349
Holtzman, J. A., et al. 1995, PASP, 107, 156
Hunter, D. A. 1994, AJ, 107, 565
Johnson, K. E., Leitherer, C., Vacca, W. D., & Conti, P. S. 2000, AJ, 120, 1273
Kennicutt, R. C., Jr., & Hodge, P. W. 1986, ApJ, 306, 130
Lasker, B. M. 1977, ApJ, 212, 390
Lucke, P. B., & Hodge, P. W. 1970, AJ, 75, 171
McKee, C. F., Van Buren, D., & Lazareff, B. 1984, ApJ, 278, L115
Norman, C. A., & Ferrara, A. 1996, ApJ, 467, 280
Oey, M. S. 1996, ApJ, 467, 666
Oey, M. S., & Massey, P. 1994, ApJ, 425, 635
———. 1995, ApJ, 452, 210
Osterbrock, D. E., Fulbright, J. P., Martel, A. R., Keane, M. J., Trager, S. C., & Basri, G. 1996, PASP, 108, 277
Panagia, N. 1973, AJ, 78, 929
Peimbert, M., Rayo, J. F., & Torres-Peimbert, S. 1975, Rev. Mexicana Astron. Astrofiz., 1, 289
Prinja, R. K., Barlow, M. J., & Howarth, I. D. 1990, ApJ, 361, 607
Rosado, M., Georgelin, Y. M., Georgelin, Y. P., Laval, A., & Monnet, G. 1982, A&A, 115, 61
Saken, J. M., Shull, J. M., Garmany, C. D., Nichols-Bohlin, J., & Fesen, R. A. 1992, ApJ, 397, 537
Schaerer, D., & de Koter, A. 1997, A&A, 322, 598
Scowen, P. A., et al. 1998, AJ, 116, 163
Spyromilio, J. 1995, MNRAS, 277, L59
Stasińska, G., & Schaerer, D. 1997, A&A, 322, 615
Strickland, D. K., Heckman, T. M., Weaver, K. A., & Dahlem, M. 2000, AJ, 120, 2965
Treffers, R. R., & Chu, Y.-H. 1982, ApJ, 254, 569
Vacca, W. D., Garmany, C. D., & Shull, J. M. 1996, ApJ, 460, 914
Wang, Q. D., & Helfand, D. J. 1991, ApJ, 373, 497
Weaver, R., McCray, R., Castor, J., Shapiro, P., & Moore, R. 1977, ApJ, 218, 377
Weis, K., & Duschl, W. J. 1999, in IAU Symp. 190, New Views of the Magellanic Clouds, ed. Y.-H. Chu, N. Suntzeff, J. Hesser, & D. Bohlender (San Francisco: ASP), 134
Williams, R. J. R., Ward-Thompson, D., & Whitworth A. P. 2001, MNRAS, 327, 788